Physical Layer Performance of Multi-Band Optical Line Systems Using Raman Amplification

Physical Layer Performance of Multi-Band Optical Line Systems Using Raman Amplification

M. Cantono, *Student Member, OSA, IEEE*, A. Ferrari, *Student Member, OSA*, D. Pilori, *Student Member, OSA*,E. Virgillito, *Student Member, OSA*, J.L. Auge, *Member, OSA*, and V. Curri, *Member, IEEE*

***Abstract*—Network operators are aiming at overcoming the envisioned data traffic crunch by relying on the already installed fiber cables. So, multi-band optical line systems will be the solution, starting from the extension to the C+L band transmission. Such a bandwidth extension is also speeding up network disaggregation to avoid an increase in costs. Thus, line system (LS) controllers need Quality-of-Transmission Estimator (QoT-E) modules able to quickly estimate the merit of lighpaths, so analytical models for the transmission layer are mandatory. We review the generalized Gaussian noise (GGN) model for wideband prediction of nonlinear interference generation and validate its accuracy by comparing C+L simulative results to model predictions. Results are obtained in case of using hybrid Raman and Erbium Doped Fiber Amplifier (EDFA) amplification and display an excellent conservative accuracy. We also present an experimental validation done on commercial equipment that confirms how the GGN-model is the most feasible solution for QoT-E modules in multi-band LS controllers, enabling a frequency-resolved minimization of system margins.**

***Index Terms*—Optical Line System, NLI, GGN-model, QoT-E, Stimulated Raman Scattering, Multi-Band Optical System**

I. Introduction

QUALITY of transmission (QoT) estimation is a pivotal element to successfully deploying disaggregated multi-vendor optical networks. Such a request is driven by network operators that have recently started to install white boxes in their backbone infrastructure to lower network costs and to speed up cycles of technology upgrades. However, to make full network disaggregation a consolidated reality, operators require device interoperability without losing performance, i.e., capacity and reliability. Interoperability is needed to make network elements from different vendors work together in a unique infrastructure with reduced operational and control complexity. To tackle this problem, open models for network elements to be integrated into off-the-shelf software defined controllers have been proposed by consortia of operators such as the Telecom Infra Project (TIP) [1], Open-ROADM [2] and OpenConfig [3]. To this aim, vendor agnostic QoT estimators (QoT-Es) are needed to design and optimize disaggregated network architectures. QoT-Es enable line system (LS) controllers and orchestrators to rely on a quick-yet-accurate lightpath (LP) feasibility calculation. To this end, some of the previously mentioned consortia are spending large efforts to develop such QoT-Es. Furthermore, as operators require quick-yet-accurate QoT-E modules, performance predictions via numerical solutions of the nonlinear Shrödinger equation are not feasible, therefore analytical models for performance estimation are usually adopted. Such models need to account for the two major propagation impairments in optical communication systems, i.e., amplified spontaneous emission (ASE) noise generated by optical amplifiers, and nonlinear impairments caused by the nonlinear Kerr effect [4].

For state-of-the-art transmission techniques based on multi-level modulation formats exploiting polarization-division multiplexing with DSP-operated coherent receivers, it has been widely shown that nonlinear impairments can be well summarized by the accumulation of a noise-like Gaussian-distributed disturbance named nonlinear interference (NLI) [5]–[11]. This is also the case with systems exploiting bandwidths exceeding the C-band and with strong polarization mode dispersion (PMD) [12]–[15]. Therefore, the QoT metric that takes into account these two effects is represented by the generalized or effective signal-to-noise ratio (SNR) [5], [6] considering both the accumulated ASE noise and NLI. The SNR is indeed the metric determining the bit error rate (BER), given the modulation format. Several analytical models to accurately estimate the NLI accumulation noise have been proposed in literature and extensively validated by experimental results [6], [7], [9]–[11], [16]–[18]. The Gaussian Noise (GN) model [6], [7] with incoherent NLI accumulation is the most widely adopted model as it represents an effective tool to get quick and accurate conservative predictions of NLI, and it has been successfully validated in commercial systems over the C-band [19], [20].

The continuous growth in data traffic [21] is pushing vendors and operators to explore new optical transmission technologies to overcome a possible capacity crunch in backbone networks [22]. A firm requirement is on the use of already installed cables to maximize CAPEX returns. Thus, exploiting the optical transmission bandwidth beyond the conventional C-band is the proposed solution to achieve this goal [23]. Nowadays, C+L LSs enabling 200 LPs on the 50 GHz Dense Wavelength Division Multiplexing (WDM) grid are gaining traction, and commercial systems with these characteristics are already available on the market [24]. In such a novel transmission scenario, the interplay of nonlinear propagation effects with wideband phenomena – mainly Stimulated Raman Scattering (SRS) – needs to be understood, and the joint impairments properly addressed in QoT-Es. SRS enables a power transfer from higher- to lower-frequency spectral re-

Mattia Cantono, Alessio Ferrari, Dario Pilori, Emanuele Virgillito and Vittorio Curri are with DET, Politecnico di Torino, 1029 Torino (TO), Italy. E-mail: mattia.cantono@polito.it)

Jean-Luc Auge is with Orange Labs, France. E-mail: jean-luc.auge@orange.com.

gions with a maximum efficiency roughly at 100 nm (13 THz) of spectral separation. So, the spectral tilt across the WDM channel comb may induce considerable effects when the entire C+L bandwidth – 1530 to 1625 nm – is exploited, as different channels undergo different loss/gain profile as a function both of the propagation distance z and the spectral axis f. SRS also enables distributed amplification – Raman amplifiers (RA) – by using depolarized high power pumps, co- or counter-propagating, with LP carrying data traffic [25]. RAs are extensively used for the L-band either as unique amplification method or together with EDFA to implement hybrid Raman-Erbium amplifiers. RA exacerbates the interplay of nonlinear effects with gain/loss variations with z and f because it induces a frequency-dependent distributed power enhancement.

The GN-model has been extended to include distributed amplification [26], [27], but the joint effects of frequency and space variations were not fully addressed. Recently, the generalized Gaussian noise (GGN) model has been proposed [28], [29] to model how spatially and frequency distributed power variations affect the generation of NLI. The GGN-model has been experimentally validated in [28], [30] and compared to other approaches to NLI modeling, including the GN-model.

In this paper, we extend the results presented in [30] by performing the additional analyses, mainly considering Raman amplification. We compare the GN- vs. the GGN-model accuracy for estimating the QoT of C+L line systems including hybrid Erbium-Raman amplifiers using full split step simulations as reference. In Sec. II, the GN- and GGN-model for NLI prediction are reviewed. In Sec. III, for the first time to the best of authors' knowledge, we show how the GGN-model is a conservative option for frequency-resolved NLI modeling over the entire C+L bandwidth, so enabling a multi-band QoT-E. In Sec. IV, we present a comparison over the experimental setup of [30], relying on a number of measured points increased from 3 to 7 across the WDM spectrum that better show the need for the GGN-model for NLI prediction, also in case of larger uncertainties, as in experimental scenarios. Finally, in Sec. V conclusions are drawn and future evolution is addressed.

II. Wideband NLI Modeling Approaches for QoT-E

The QoT-metric, i.e. the signal-to-noise-ratio (SNR), is the key parameter to evaluate the overall performance of the physical layer and it is composed of a linear factor, which takes into account the ASE noise and a nonlinear one quantifying the NLI. These two phenomena are quantified by the linear signal-to-noise ratio ($\mathrm{SNR_{LIN}}$) for ASE noise and the nonlinear SNR ($\mathrm{SNR_{NLI}}$) for the NLI. These quantities can be combined together to get the generalized SNR as reported in (1).

$$\mathrm{SNR} = \left[\frac{1}{\mathrm{SNR_{LIN}}} + \frac{1}{\mathrm{SNR_{NLI}}}\right]^{-1} \tag{1}$$

The linear SNR is calculated taking into account ASE noise generated by each amplifier. Thus, it can be computed as follows:

$$\mathrm{SNR_{LIN}} = \frac{P_{\mathrm{ch}}}{P_{\mathrm{ASE}}} = \frac{P_{\mathrm{ch}}}{\mathrm{NF}hf(G-1)B} \tag{2}$$

In this equation, P_{ch} is the per-channel power and P_{ASE} is ASE noise power, NF is the amplifier noise figure, h is the Planck constant, G is the amplifier gain, B is the reference bandwidth and f is the frequency at which P_{ASE} is evaluated. The nonlinear SNR, instead, can be expressed as:

$$\mathrm{SNR_{NLI}} = \frac{P_{\mathrm{ch}}}{P_{\mathrm{NLI}}} = \frac{P_{\mathrm{ch}}}{P_{\mathrm{NLI}}} = \frac{P_{\mathrm{ch}}}{\int_{B_{\mathrm{ch}}} G_{\mathrm{NLI}}(f)\,\mathrm{d}f} \tag{3}$$

where P_{NLI} is the equivalent power of the nonlinear disturbances and it can be computed by integrating the power spectral density of the NLI, $G_{\mathrm{NLI}}(f)$, on the signal frequency slot B_{ch}. As discussed in the introduction, several models have been proposed to compute $G_{\mathrm{NLI}}(f)$. For this work, we will model NLI noise by means of the GN model [7] and its generalized version – the GGN – (proposed in [29], [31], [32]). The GGN model formula is reported in (4), where γ is the fiber nonlinear coefficient, $G_{\mathrm{TX}}(f)$ is the transmitted power spectral density in $z = 0$, β_2 and β_3 are the dispersion coefficients, L_s is the span length and $\rho(z, f)$ is the overall signal gain/loss which takes into account both the fiber attenuation and the stimulated Raman scattering along the fiber vs. propagation distance z and frequency f.

III. Simulative Investigation

In this section, the GN and GGN models are compared over a simulation of a wideband C+L transmission link with hybrid EDFA-Raman amplification. Simulations are performed by solving the nonlinear Schrödinger equation via full time-domain split-step Fourier method with the FFSS library as described in [33].

A. System setup

A high-level schematic of the simulated setup is shown in Fig. 1. The system transmits 161 WDM channels in the 50-GHz DWDM grid, divided among the C-band (83 channels) and L-band (78 channels). Between the two bands, there is a 300-GHz guardband, which makes the total optical bandwidth

$$G_{\mathrm{NLI}}(L_s, f) = \frac{16}{27}\gamma^2\rho(L_s, f)^2 \iint_{-\infty}^{+\infty} G_{\mathrm{TX}}(f_1)G_{\mathrm{TX}}(f_2)G_{\mathrm{TX}}(f_1+f_2-f) \left|\int_0^{L_s} \exp(+j4\pi^2(f_1-f)(f_2-f)[\beta_2+\pi\beta_3(f_1+f_2)]\zeta)\frac{\rho(\zeta,f_1)\rho(\zeta,f_1+f_2-f)\rho(\zeta,f_2)}{\rho(\zeta,f)}\mathrm{d}\zeta\right|^2 \mathrm{d}f_1\mathrm{d}f_2 \tag{4}$$

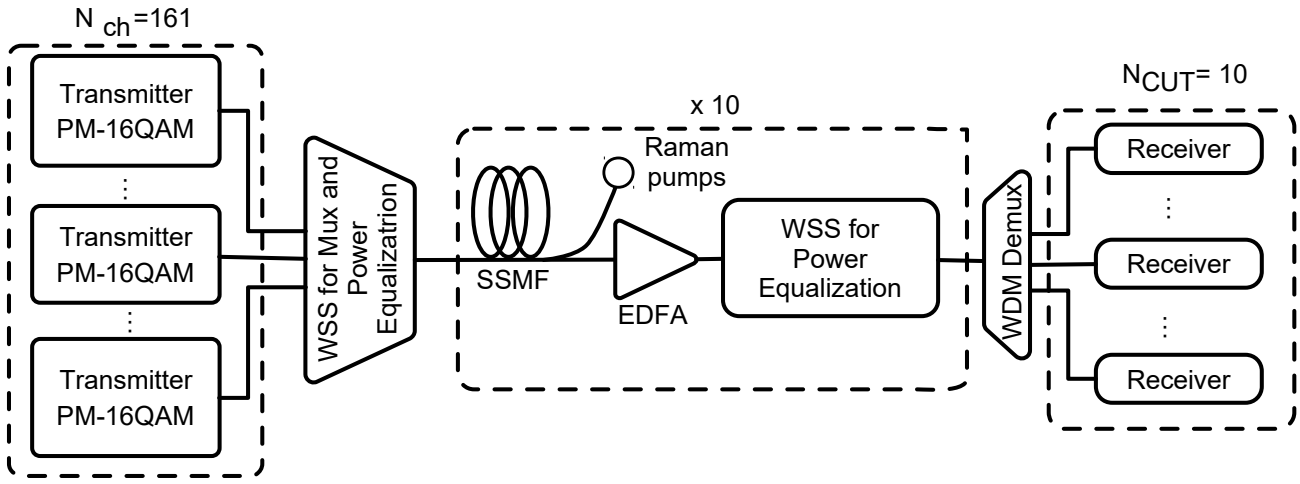

Figure 1. Simulation setup.

Table I
SIMULATED FIBER PARAMETERS

Parameter	Value
Span length	$L_s = 80$ km
Maximum number of spans	$N_s = 10$
Chromatic dispersion	$D = 16.7$ ps/nm/km
Nonlinear coefficient	$\gamma = 1.3$ 1/W/km
Polarization Averaged Raman Coefficient	$C_r = 0.39$ 1/W/km
Polynomial coefficients of $\alpha(f)$ around $f_0 = 193.6$ THz	$\alpha_0 = 0.19$ dB/km $\alpha_1 = 5.97 \times 10^{-5}$ dB/km/THz $\alpha_2 = 8.3 \times 10^{-4}$ dB/km/THz^2

Table II
RAMAN AMPLIFIER PUMP CONFIGURATIONS

Frequency (THz)	Power (mW)
201.07	250
202.43	300
203.11	150
203.80	150
204.50	150

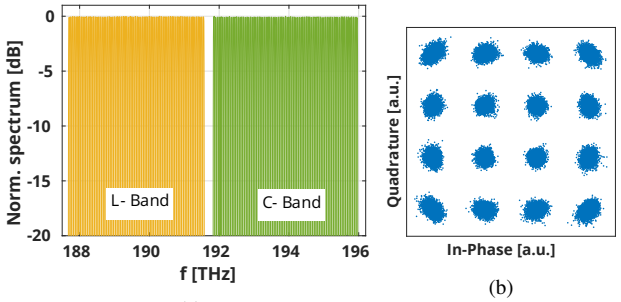

(a) (b)

Figure 2. Simulation transmitted C+L spectrum (a) and received constellation after 10 spans (b). L-band channels are depicted in yellow, while C-band channels are depicted in green.

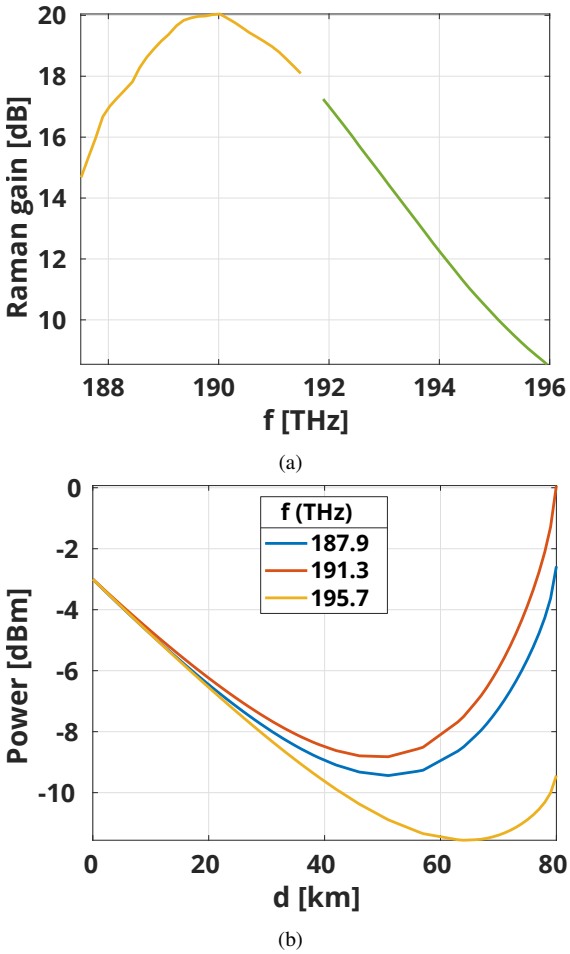

Figure 3. (Top): Raman gain, taking into account SRS from pumps and signal, at the end of the 80-km span. C-band is depicted in green, while L-band is depicted in yellow. (Bottom): Power evolution across each span of three different WDM channels.

equal to 8.3 THz. Fig. 2a shows the normalized optical spectrum of the transmitted signal, divided into the C- (green) and L-band (yellow).

Each WDM channel is modulated with a 32-GBaud PM-16QAM signal with 15-% roll-off root raised cosine spectrum,

and it is propagated through 10 spans 80-km long of single mode fiber (SMF), whose parameters are summarized in table I. Given the large transmission bandwidth, attenuation was not considered constant for all frequencies, but it changed according to

$$\alpha(f) = \alpha_0 + \alpha_1(f - f_0) + \frac{1}{2}\alpha_2(f - f_0)^2 \quad [\text{dB/km}] \quad (4)$$

with parameters summarized in table I. Since the simulation of dispersion slope introduces considerable computational overheads, we did not include such feature in our analysis. Nevertheless, its impact on NLI generation in the considered scenario is limited within 0.4 dB of estimated extra NLI [34].

For this particular scenario, we considered a flat transmitted WDM spectrum, with a per-channel transmitted power of -3 dBm, which gives a total launch power of $+19.1$ dBm. At the end of each span, an ideal (without insertion loss) Wavelength Selective Switch (WSS) equalizes the per-channel power to recover the original transmitted spectrum.

Amplification is achieved using counter-propagating Raman pumps and an EDFA amplifier with 4-dB noise figure. Frequency and power of the pumps are shown on Table II. The Raman gain at end of each span generated by the SRS interaction between the pumps and the signal is shown on Fig. 3a. Notice that the Raman gain is non flat across the frequency spectrum, with an average tilt of ~ 8 dB. We assume that EDFA and WSS are able to recover for the remaining span loss and equalize the channel powers to achieve span transparency, i.e. the power spectral density of the signal at the beginning of each span is always constant. Given the typical required SNR for PM-16QAM, interactions between ASE noise and NLI are negligible [18]. Therefore, to simplify the simulation, ASE noise was not added in-line, but it was added at the receiver, taking into account both EDFA noise figure and the effective noise figure of Raman amplification.

Fig. 3b shows the power evolution of three channels spread across the WDM comb, highlighting how different frequencies undergo different power variations. For all channels, first, power decreases due to fiber attenuation, then, towards the end of the span, it increases due to the effect of Raman pumps. L-band channels achieve transparency. The C-band channel, instead, does not fully achieve transparency, as they get depleted by SRS, transferring power to the L-band channels.

At the receiver, 10 channels-under-test (CUT), spaced across the full WDM spectrum, are filtered and received with a coherent receiver. The frequencies of the CUT are $f_0 = \begin{bmatrix}187.7 & 189.65 & 191.55 & 191.85 & 193.9 & 195.95\end{bmatrix}$ THz. The CUT are generated with 6 repetitions of different 2^{14} PRBS sequences, while the other channels are generated with random PM-16QAM symbols. The receiver uses a fully-data-aided 17-tap fractionally-spaced LMS adaptive equalizer, followed by the evaluation of the SNR directly on the received constellation.

An example of a received constellation, without ASE noise, is shown in Fig. 2b. Since lasers are assumed ideal, no phase recovery is applied, which explains the slight amount of phase noise that is caused by NLI. Nevertheless, in presence of ASE noise, this small phase noise does not significantly change noise statistics, keeping reliable the SNR estimation on the constellation [18].

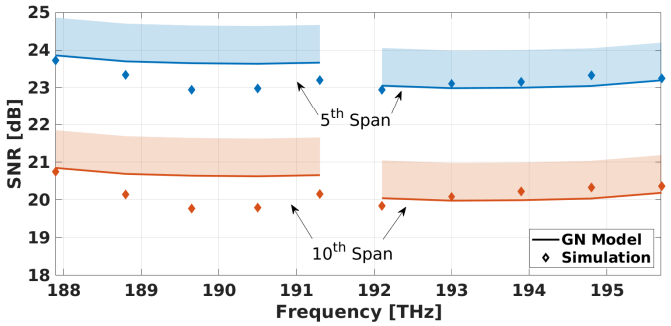

Figure 4. Comparison of simulation results vs GN model estimation after 5 spans (blue) and after 10 spans (red).

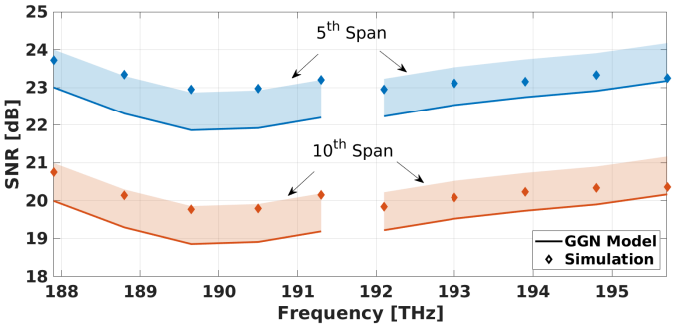

Figure 5. Comparison of simulation results vs GGN model estimation after 5 spans (blue) and after 10 spans (red).

B. Results and discussion

Fig. 4 and Fig. 5 compare the SNR resulting from the numerical simulation against estimations computed using both the GN model (Fig. 4) and the GGN model (Fig. 5). Diamond dots of Fig.4 and Fig. 5 show simulation results, while continuous lines represent model predictions. Light color bars represent 1-dB margin, which are positive-only since the GN model slightly overestimate NLI power [7] due to its signal Gaussianity hypothesis, making GN model-based non-linear SNR predictions conservative.

All the results are reported after 5 and 10 spans, in blue and red, respectively. Results show higher NLI in the L-band with respect to the C-band. This is due to SRS, causing the L-band channels to experience less attenuation than C-band channels, enlarging their power and thus, enhancing NLI generation. On the other end, ASE noise is higher in the C-band with respect to L-band, "balancing" the difference in NLI. This effect is due to the difference in effective noise figure of Raman and EDFA amplification.

Comparing GN and GGN predictions, GN model predictions are close to the simulation results, especially in the C-Band (as shown in Fig. 4). However, the GN model does not predict the correct frequency dependence of the SNR due to Raman effects. Furthermore, even if it overestimates NLI power, it is conservative only in the C-band, while, in the L-Band, NLI is *underestimated*. This is due to the fact that

the GN model does not take into account any frequency/space distributed variation of power levels along the fiber. On the contrary, the GGN model, shown in Fig. 5, gives a good and conservative prediction on the SNR across the full WDM comb, and all results are inside the 1 dB margins. Most importantly, the GGN model properly predicts the shape of the SNR variation across the spectrum, delivering consistent QoT estimations across the full channel comb. Notice also that, for both GN and GGN models, simulation results are closer to model predictions for the 10 spans case, as the signal gets closer to being Gaussian-distributed due to chromatic dispersion.

IV. Experimental Investigation

After comparing the GN and the GGN-models in the fully-controlled environment of numerical simulations, in this section the same comparison will be performed in an experimental setup with commercial transponders. We remark that, in the context of numerical simulations, any mismatch between simulations and models is caused by modeling inaccuracies. On the other hand, in real world experiments, inaccuracies between model predictions and actual measured performance can be attributed to several factors, including:

- Lack of knowledge of system parameters (e.g. actual fiber parameters for each fiber of the setup, amplifier working points etc.);
- Uncertainties associated with measurement procedures and equipment;
- Modeling inaccuracies (e.g. simplified modeling hypotheses);

All these effects are jointly affecting the estimations and measurements, therefore when comparing analytical predictions and measurements, an uncertainty bar needs to be considered. In the results presented later, such uncertainty bar is set around ± 0.25 dB around a baseline modeling estimation.

A. Experimental Setup

Fig. 6 shows the experimental setup, which is the Orange laboratory test-bed, typically used for the performance evaluation of the transponders deployed in Orange networks, consisting of 20 spans of 80-km Corning SMF-28e+® optical fiber.

58 WDM channels in the C-band were transmitted, and 3 of them are the CUT, modulated by 32-Gbaud 100-Gb/s PM-QPSK current-generation commercial transponders. The remaining 55 channels are generated from several lasers modulated by two 28 GBaud 100-Gb/s PM-QPSK laboratory transmitters, modulating alternatively odd and even interfering channels. At the transmitter, a WSS is used to combine the CUT and interfering channels over the standard 50 GHz DWDM grid and 2 additional equalizers are used during transmission every 6 spans to equalize the power of the channels. No amplifier pre-tilt or WSS pre-emphasis is applied, in order to exacerbate the effect of SRS.

Real-time measurements of pre-FEC Q-factor were performed on the three CUT. To measure more than three channels, the transponders were tuned over 7 different frequencies $[192.95; 193.35; 193.65; 194.00; 194.35; 194.75; 195.15]$ THz so that the Q-factor is evaluated uniformly across the C-band. In order to map the measured Q-factors to the generalized SNR, the back-to-back curve is characterized for every transponder over each of the 7 frequencies under test at a constant received power of -17 dBm.

B. Experimental Results

The WDM channel comb was propagated through the 20×80 km link, and the power excursions of each channel at the end of each span was recorded exploiting the amplifier monitoring port and an Optical Spectrum Analyzer (OSA) (Fig. 7). Similarly, the linear SNR at the end of each amplifier was measured. The total optical launch power was set to 18 dBm, corresponding to 0.4 dBm per channel. The power evolution of all the WDM channels along the first six spans are depicted in Fig. 7a. In addition to this, the power variations for 3 of the channels under test along the full link are represented in Fig. 7b: the linear tilt (in dB) induced by SRS is evident. Amplifier ripple is clearly visible on side channels as a nonlinear power excursion added on top of the linear SRS-induced tilt.

We compare the GN and the GGN model for QoT estimation without exploiting the exactly measured power profiles for the WDM channel at the input of each fiber. Instead, we just consider the nominal launch power value per channel, i.e. 0.4 dBm. We assume all fibers to have a 0.75 dB connector loss. We consider Corning SMF-28e+® datasheet fiber parameter values to compute the nonlinear SNR. We exploit the linear SNR measurement at the end of each fiber span to compute the generalized SNR. Thus, the only term of (1) that is modeled in the next comparisons is related to the nonlinear SNR. Using the aforementioned reference values for power settings and fiber parameters, we compute a nominal SNR curve for the 7 channels under test.

We purposely consider nominal launch power levels to test the validity of these models in the context of QoT estimation for network operations, where only nominal channel power values are often accessible. To take into account the errors and uncertainties associated to both modeling and experimental measurements, an uncertainty region of ± 0.25 dB around the model predictions is set: if experimental measurements fall inside this region, they should be considered good.

Results are depicted in Fig. 8 and Fig. 9. Fig. 8 shows the experimental results and the SNR predictions obtained with the GN model. Fig. 9 shows the GGN-model predictions. Comparing Fig. 8 and Fig. 9, it is immediately clear that the GGN model is able to well predict QoT performance across the full WDM comb. The GN model based prediction is good in the middle of the WDM comb, but fails to obtain reliable estimations away from it. This is evident especially for low frequency channels for which the GN model overestimates performance by ~ 0.8 dB. In the higher frequency portion of the WDM spectrum, the estimation is good, as high frequency channels are depleted by SRS, thus they are limited by ASE noise: prediction errors in NLI noise are not as relevant there, as NLI is negligible when compared to linear noise.

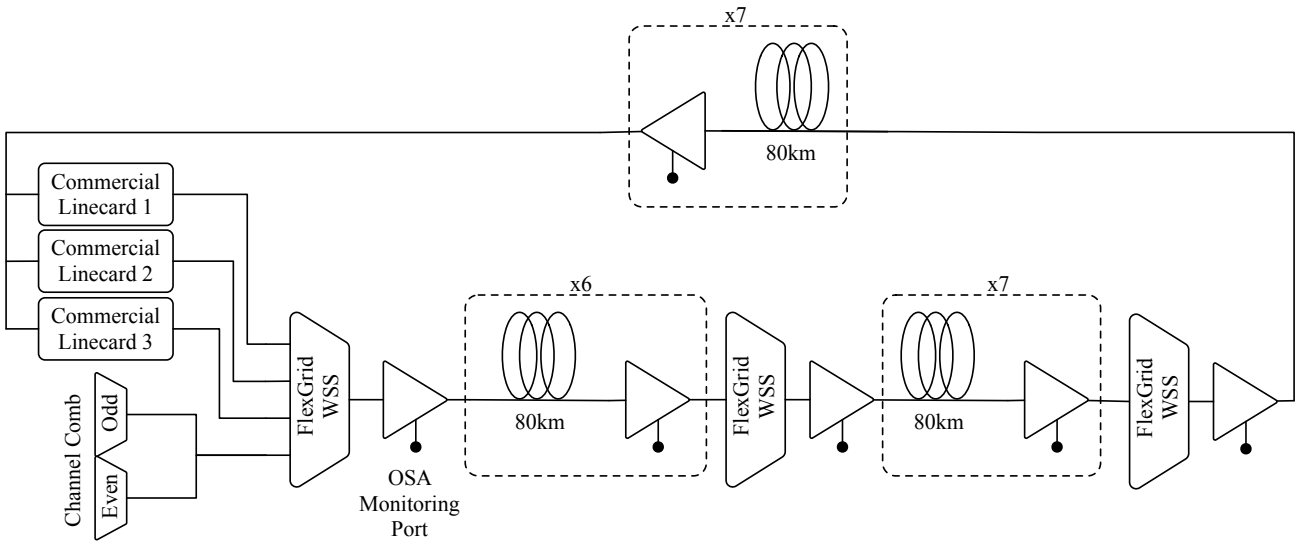

Figure 6. Orange Lab testbed and setup used for experimental validation of the GGN-model.

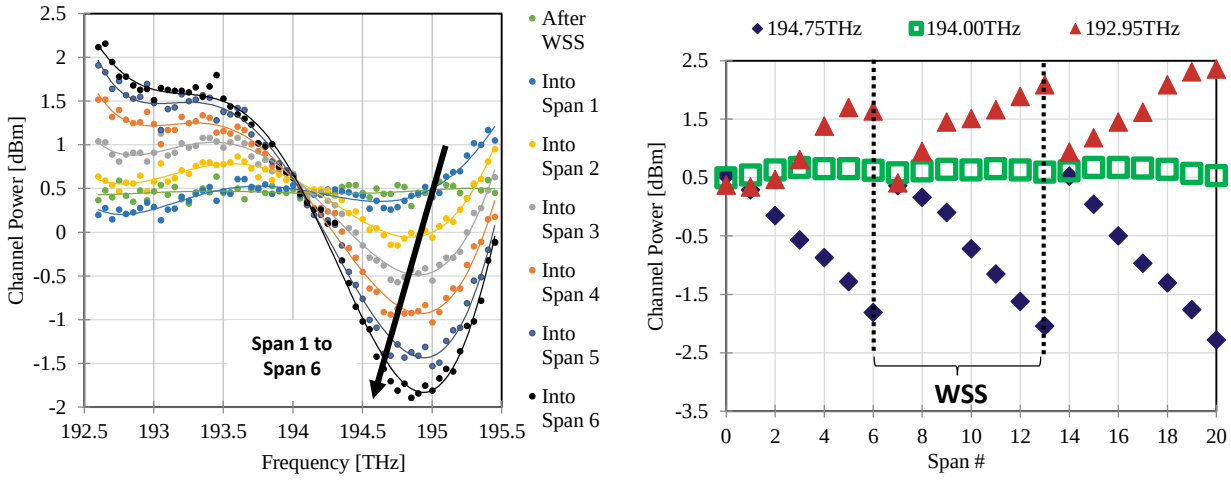

(a) (b)

Figure 7. Power evolution due to SRS and amplifier ripple along the Orange testbed. (a) Channels power excursion for the first 6 spans over the Orange testbed. Linear tilt due SRS and a superimposed gain ripple are clearly visible. (b) Power per channel evolution for three channels (blue, green and red) at the beginning of each span.

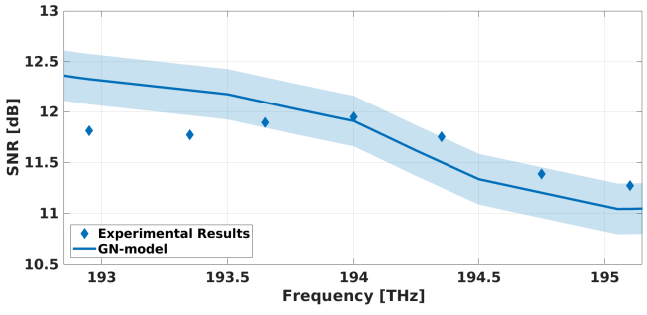

Figure 8. Comparison of experimental results vs GN model based estimations.

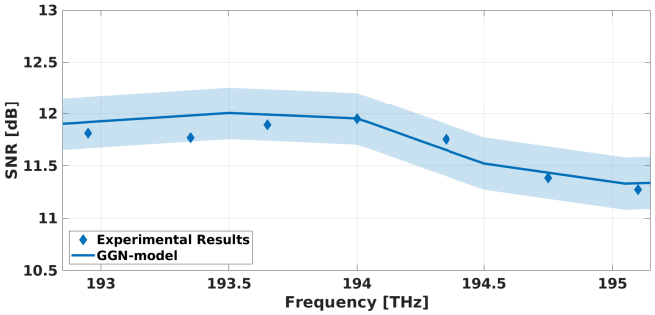

Figure 9. Comparison of experimental results vs GGN model based estimations.

On the other hand, the GGN model correctly evaluates the slope of the SNR values vs frequency. The gap between nominal prediction curve and experimental measurements is smaller than 0.25 dB for all points. The 193.35 THz channel

shows the larger error as amplifier ripple is more significant there, and using the nominal power levels for QoT estimations yields larger inaccuracies. It should also be highlighted that, in this scenario, the GGN-model estimations are not conservative with respect to experimental data, due to the aforementioned system parameters uncertainty eroding the conservative margin that was evident in simulation results presented in Sec. III. Fig. 9 shows that the GGN model enables reliable estimation of QoT performance across the full WDM comb by correctly taking into account the interplay between SRS and NLI generation.

V. Comments and Conclusions

We have addressed the problem of estimating the transmission merit of lighpaths in disaggregated multi-vendor networks relying on optical line systems deploying multi-band transmission and possibly Raman amplification. We have extended the results presented in [30] by comparing the predictions of the GN-model to the GGN-model's for NLI evaluation using as a reference simulative results for a C+L LS deploying hybrid Raman and EDFA amplification. Results confirm that the choice of the GGN-model for QoT-E guarantees a conservative NLI evaluation on the entire C+L bandwidth with an excellent prediction of the NLI spectral slope. Thus, planning and signaling operations can be performed with minimum margin. We have also presented a comparison of models' predictions over the experimental setup of [30], displaying a number of measured points increased from 3 to 7 over the transmission band. Also the experimental results performed over a limited bandwidth and without Raman amplification show the need for the GGN-model in QoT-E to implement frequency-resolved and reliable performance estimation in a multi-vendor context of disaggregated network.

Acknowledgment

The authors would like to thank Synopsys Inc. for supplying the OptSim software used to evaluate the Raman gain profile of the simulation. The authors would also like to thank Clara Catanese and Jordane Thouras from Orange labs for the support in performing the experimental measurements.

References

[1] TIP. The Telecom Infra Project (TIP). [Online]. Available: https://telecominfraproject.com

[2] O. ROADM. Open ROADM MSA. [Online]. Available: http://www.openroadm.org

[3] OpenConfig. OpenConfig. [Online]. Available: http://openconfig.net/

[4] G. P. Agrawal, *Fiber-Optic Communication Systems*, 4th ed., ser. Wiley series in microwave and optical engineering. Wiley, 2010, oCLC: 705930760.

[5] F. Vacondio, O. Rival, C. Simonneau, E. Grellier, A. Bononi, L. Lorcy, J.-C. Antona, and S. Bigo, "On nonlinear distortions of highly dispersive optical coherent systems," *Optics Express*, vol. 20, no. 2, p. 1022, 2012. [Online]. Available: https://www.osapublishing.org/oe/abstract.cfm?uri=oe-20-2-1022

[6] A. Carena, V. Curri, G. Bosco, P. Poggiolini, and F. Forghieri, "Modeling of the Impact of Nonlinear Propagation Effects in Uncompensated Optical Coherent Transmission Links," *Journal of Lightwave Technology*, vol. 30, no. 10, pp. 1524–1539, 2012. [Online]. Available: http://ieeexplore.ieee.org/document/6158564/

[7] P. Poggiolini, G. Bosco, A. Carena, V. Curri, Y. Jiang, and F. Forghieri, "The GN-Model of Fiber Non-Linear Propagation and its Applications," *Journal of Lightwave Technology*, vol. 32, no. 4, pp. 694–721, 2014. [Online]. Available: http://ieeexplore.ieee.org/document/6685826/

[8] P. Serena and A. Bononi, "An Alternative Approach to the Gaussian Noise Model and its System Implications," *Journal of Lightwave Technology*, vol. 31, no. 22, pp. 3489–3499, 2013. [Online]. Available: http://ieeexplore.ieee.org/document/6621015/

[9] M. Secondini and E. Forestieri, "Analytical Fiber-Optic Channel Model in the Presence of Cross-Phase Modulation," *IEEE Photonics Technology Letters*, vol. 24, no. 22, pp. 2016–2019, 2012. [Online]. Available: http://ieeexplore.ieee.org/document/6297443/

[10] P. Johannisson and M. Karlsson, "Perturbation Analysis of Nonlinear Propagation in a Strongly Dispersive Optical Communication System," *Journal of Lightwave Technology*, vol. 31, no. 8, pp. 1273–1282, 2013. [Online]. Available: http://ieeexplore.ieee.org/document/6459512/

[11] R. Dar, M. Feder, A. Mecozzi, and M. Shtaif, "Properties of nonlinear noise in long, dispersion-uncompensated fiber links," *Optics Express*, vol. 21, no. 22, p. 25685, 2013. [Online]. Available: https://www.osapublishing.org/oe/abstract.cfm?uri=oe-21-22-25685

[12] R. Pastorelli, G. Bosco, A. Carena, P. Poggiolini, V. Curri, S. Piciaccia, and F. Forghieri, "Investigation of the Dependence of Non-Linear Interference on the Number of WDM Channels in Coherent Optical Networks," in *2012 38th European Conference and Exhibition on Optical Communications*. OSA, 2012, p. We.2.C.2. [Online]. Available: https://www.osapublishing.org/abstract.cfm?uri=ECEOC-2012-We.2.C.2

[13] D. J. Elson, G. Saavedra, K. Shi, D. Semrau, L. Galdino, R. Killey, B. C. Thomsen, and P. Bayvel, "Investigation of bandwidth loading in optical fibre transmission using amplified spontaneous emission noise," *Optics Express*, vol. 25, no. 16, p. 19529, 2017. [Online]. Available: https://www.osapublishing.org/abstract.cfm?URI=oe-25-16-19529

[14] G. Saavedra, M. Tan, D. J. Elson, L. Galdino, D. Semrau, M. A. Iqbal, I. Phillips, P. Harper, N. MacSuibhne, A. Ellis, D. Lavery, B. C. Thomsen, R. Killey, and P. Bayvel, "Experimental Investigation of Nonlinear Signal Distortions in Ultra-Wideband Transmission Systems," in *2017 Optical Fiber Communication Conference*. OSA, 2017, p. W1G.1. [Online]. Available: https://www.osapublishing.org/abstract.cfm?URI=OFC-2017-W1G.1

[15] M. Cantono, D. Pilori, A. Ferrari, A. Carena, and V. Curri, "Observing the Interaction of PMD with Generation of NLI in Uncompensated Am- plified Optical Links," in *2018 Optical Fiber Communications Conference and Exhibition (OFC)*, 2018, pp. 1–3.

[16] A. Mecozzi and R.-J. Essiambre, "Nonlinear Shannon Limit in Pseudolinear Coherent Systems," *Journal of Lightwave Technology*, vol. 30, no. 12, pp. 2011–2024, 2012. [Online]. Available: http://ieeexplore.ieee.org/document/6175093/

[17] A. Bononi, P. Serena, N. Rossi, E. Grellier, and F. Vacondio, "Modeling nonlinearity in coherent transmissions with dominant intrachannel-four-wave-mixing," *Optics Express*, vol. 20, no. 7, p. 7777, 2012. [Online]. Available: https://www.osapublishing.org/oe/abstract.cfm?uri=oe-20-7-7777

[18] P. Poggiolini and Y. Jiang, "Recent Advances in the Modeling of the Impact of Nonlinear Fiber Propagation Effects on Uncompensated Coherent Transmission Systems," *Journal of Lightwave Technology*, vol. 35, no. 3, pp. 458–480, 2017. [Online]. Available: http://ieeexplore.ieee.org/document/7577767/

[19] G. Grammel, V. Curri, and J. L. Auge, "Physical Simulation Environment of The Telecommunications Infrastructure Project (TIP)," in *2018 Optical Fiber Communication Conference*, 2018.

[20] M. Filer, M. Cantono, A. Ferrari, G. Grammel, G. Galimberti, and V. Curri, "Multi-vendor experimental validation of an open source QoT estimator for optical networks," *J. Lightwave Technol.*, vol. 36, no. 15, pp. 3073–3082, Aug 2018.

[21] Cisco, "Cisco Visual Networking Index: Forecast and Methodology, 2016–2021." [Online]. Available: https://www.cisco.com/c/en/us/solutions/collateral/service-provider/visual-networking-index-vni/complete-white-paper-c11-481360.pdf

[22] P. J. Winzer and D. T. Neilson, "From Scaling Disparities to Integrated Parallelism: A Decathlon for a Decade," *Journal of Lightwave Technology*, vol. 35, no. 5, pp. 1099–1115, 2017.

[23] G. Rizzelli, G. Maier, M. Quagliotti, M. Schiano, and A. Pattavina, "Assessing the Scalability of Next-Generation Wavelength Switched Optical Networks," *Journal of Lightwave Technology*, vol. 32, no. 12, pp. 2263–2270, June 2014.

[24] S. Hardy. Nokia upgrades 1830 PSS packet-optical transport family with new coherent chipsets, improved multi-rate performance. [Online]. Available: http://bit.ly/2zLYTv0

[25] M. Islam, "Raman amplifiers for telecommunications," *IEEE Journal of Selected Topics in Quantum Electronics*, vol. 8, no. 3, pp. 548–559, 2002. [Online]. Available: http://ieeexplore.ieee.org/document/1016358/

[26] P. P. G. B. Vittorio Curri, Andrea Carena and F. Forghieri, "Extension and validation of the gn model for non-linear interference to uncompensated links using raman amplification," *Optics Express*, vol. 21, no. 3, pp. 3308–3317, 2013. [Online]. Available: https://www.osapublishing.org/oe/abstract.cfm?uri=oe-21-3-3308

[27] A. C. Vittorio Curri, "Merit of raman pumping in uniform and uncompensated links supporting nywdm transmission," *Journal of Lightwave Technology*, vol. 34, no. 2, pp. 554–565, 2016.

[28] M. Cantono, D. Pilori, A. Ferrari, C. Catanese, J. Thouras, J. Auge, and V. Curri, "On the Interplay of Nonlinear Interference Generation with Stimulated Raman Scattering," *Journal of Lightwave Technology*, vol. 36, no. 15, pp. 3131–3141, 2018.

[29] M. Cantono, D. Pilori, A. Ferrari, and V. Curri, "Introducing the Generalized GN-model for Nonlinear Interference Generation including space/frequency variations of loss/gain," *arXiv preprint arXiv:1710.02225*, 2017.

[30] M. Cantono, J. L. Auge, and V. Curri, "Modelling the Impact of SRS on NLI Generation in Commercial Equipment: an Experimental Investigation," in *Optical Fiber Communication Conference*. Optical Society of America, 2018, p. M1D.2. [Online]. Available: http://www.osapublishing.org/abstract.cfm?URI=OFC-2018-M1D.2

[31] I. Roberts, J. M. Kahn, J. Harley, and D. W. Boertjes, "Channel Power Optimization of WDM Systems Following Gaussian Noise Nonlinearity Model in Presence of Stimulated Raman Scattering," *Journal of Lightwave Technology*, vol. 35, no. 23, pp. 5237–5249, 2017. [Online]. Available: http://ieeexplore.ieee.org/document/8100929/

[32] D. Semrau, R. I. Killey, and P. Bayvel, "The gaussian noise model in the presence of inter-channel stimulated raman scattering," *Journal of Lightwave Technology*, vol. 36, no. 14, pp. 3046–3055, July 2018.

[33] D. Pilori, M. Cantono, A. Carena, and V. Curri, "Ffss: The fast fiber simulator software," in *Transparent Optical Networks (ICTON), 2017 19th International Conference on*. IEEE, 2017, pp. 1–4.

[34] V. Curri, A. Carena, A. Arduino, G. Bosco, P. Poggiolini, A. Nespola, and F. Forghieri, "Design strategies and merit of system parameters for uniform uncompensated links supporting nyquist-wdm transmission," *Journal of Lightwave Technology*, vol. 33, no. 18, pp. 3921–3932, 2015.